

Log Spiral of Revolution Highly Oriented Graphite Monochromator for Fluorescence X-ray Absorption Edge Fine Structure

D. Pease¹, M. Daniel¹, J. Budnick¹, A. Frenkel², and K. Pandya³

¹ Physics Department, University of Connecticut, Storrs, Connecticut

² Materials Research Laboratory, University of Illinois at Urbana-Champaign, Urbana, Illinois

³ Brookhaven National Laboratory, Upton, N.Y.

X-ray background noise is an experimental problem that must be dealt with when one determines x-ray absorption fine structure (XAFS) of dilute atomic species using the fluorescence technique. Of particular interest is scattered radiation or fluorescence emission from elements other than the element of interest. Diffraction peaks cause particular difficulty, and also fluorescence from elements occupying a position on the periodic table just to the left (Z-1) of the position of the atomic species of interest (Z). These noise sources contribute their own spectral features, which interfere with the desired XAFS signal.

Because of the above problems with background noise, the standard ion chamber - filter combination¹ is sometimes replaced by a multi-detecting element, energy-dispersive detector. For energy dispersive detectors, however, the total count rate one may obtain is often limited due to count pile up effects (saturation). We have, therefore, developed a log spiral of revolution (LSR), graphite monochromator. This detector offers advantages in applications such as detecting XAFS in the presence of diffraction peaks, or in the presence of intense fluorescence from concentrated species, which will saturate energy dispersive detectors.

A logarithmic spiral has the characteristic that all rays from a focal point meet the spiral at the same angle². One can therefore imagine a log spiral of revolution designed to monochromatize the fluorescence radiation emanating from a point focus in a fluorescence XAFS experiment. The ray bundle is not reflected to a true focus, but is concentrated into a region where photons can be detected by a non energy dispersive detector such as an ion chamber or an array of (PIN) diodes. Owing to a process recently developed in Russia whereby flexible films of highly oriented pyrolytic graphite (HOPG) can be economically deposited on

smooth surfaces³, such a monochromator becomes practical. The solid angle obtainable using a log spiral of revolution exceeds that obtainable with practical Johann crystal arrangements⁴, or Johansson bent crystals. Such a log spiral detector is not expected to be tunable; however, the HOPG covering process is economical, so that one could manufacture a series of interchangeable LSR detectors to cover the K_{α} emission lines of the first row transition metals.

Owing to the environmental importance of Cr metal, the shape of our prototype LSR is optimized for detection of Cr K XAFS. We use a Plexiglas form, which is smoothly machined into the shape of an LSR for Cr by a computer assisted lathe. The characteristics of the HOPG deposition process are such that thin layers (within a factor of two of 0.2 mm) can be molded onto smooth surfaces and will maintain a highly oriented, or low mosaic spread, configuration. As the thickness of the layers increases, so does the mosaic spread. For Cr K_{α} radiation normally incident onto carbon, one absorption length is ~ 1 mm. However, in practice, the effective penetration distance d is related to the Bragg angle and total path length through the carbon, such that for an absorption length of 1 mm, one has an attenuation length normal to the reflecting surface, d , of 0.17 mm. Thus, the manufacturing process is capable of applying HOPG layers, which are highly oriented, and of adequate thickness to give good intensity.

Fig. 1 represents one half of a two dimensional slice through a log spiral of revolution with the Bragg angle chosen to reflect Cr K fluorescence. The maximum solid angle which can be subtended by the log spiral depends on the minimum polar angle Φ_{\min} at which the active area, covered with HOPG, begins. For the log spiral we have tested, the active area begins at zero polar angle. For this choice of minimum polar angle,

the maximum polar angle Φ_{MAX} is about 30 degrees. This limit is set by the fact that the ray leaving the sample at zero polar angle and then diffracted by the HOPG is blocked by that HOPG surface which diffracts the ~ 30 degree polar angle ray. This angular range, for a log spiral of revolution, corresponds to a solid angle of $2\pi/3$, or 17% of 4π . A blocking shield shown in Fig. 1 is extended toward the sample until one attains the condition that no emitted fluorescence can directly go from the sample to the PIN diode array without first reflecting from the log spiral. A micrometer drive can be used to move the sample surface toward or away from the incoming beam to tune the detector so that a maximum intensity is obtained for the X-ray fluorescence line of interest. For some tests, we remove the blocking shield so as to compare results using direct fluorescence onto the PIN diodes with results including only fluorescent x-rays reflected from the HOPG. Our prototype LSR has a size scale such that there is a distance of 1.5 cm from the focus to the intersection between the zero polar angle ray and the spiral. Even with this small scale, our analysis shows that with a spot size of 0.5 mm^2 at the sample focus, the spread of incident Bragg angles is within the 0.4° FWHM of good quality HOPG⁵.

Initial tests were done on the X11 beamline at the National Synchrotron Light Source. This beam is not focused, and we used a beam spot which was $\sim 2 \text{ mm} \times 0.5 \text{ mm}$, by using the smallest opening of the hutch slits. We found that the rejection of V relative to Cr degraded if we attempted to increase the intensity by using a larger beam spot on the sample. Despite the non-focused conditions, we obtained promising preliminary results on a concentrated sample alloy of $\text{V}_{.5}\text{Cr}_{.5}$. The EXAFS of Cr is good quality, but the V step height, relative to the Cr, is markedly reduced by the log spiral. We also tested the performance of the LSR in rejecting Ti XAFS from V XAFS in a $\text{V}_{.50}\text{Ti}_{.50}$ alloy, data obtained by tuning to the V K_β line. This data was obtained at the focused X16C beamline at the NSLS. For the $\text{V}_{.50}\text{Ti}_{.50}$ alloy, one makes use of the fact that the V K_β energy is only 12 eV away from the Cr K_α energy, well within the resolution limit of HOPG for a LSR shape optimized for detection of Cr K_α . The rejection of V relative to Cr in $\text{Cr}_{.50}\text{V}_{.50}$ is about a factor of ten relative to the step height ratio obtained using an ion chamber, a limit which is largely determined by the relative intensity of the V K_β relative to the Cr K_α line. The data for rejection of Ti relative to V in a $\text{V}_{.50}\text{Ti}_{.50}$ alloy shows a comparable rejection ratio^{5,6}.

We tested the capability of the LSR to remove diffraction peaks from both Cr and V edges in a $\text{V}_{.80}\text{Cr}_{.15}\text{Ti}_{.05}$ alloy of interest for fusion reactor vessel wall applications. Also in another test, we found that one can tune the LSR to emphasize or minimize the Mn XAFS for a

$\text{Cr}_{.80}\text{Mn}_{.20}$ alloy. One can tune the LSR somewhat by changing the sample position plane. These results were obtained at the X16C focused beam at the NSLS and are illustrated in Figs. 2a, 2b, 2c, and 2d. The negative step at the position of the Mn edge in curve 2c is due to the removal of photons from the Cr excitation channel at the energy onset of the Mn K edge. By slightly changing the position of the sample plane, the Mn edge can be enhanced, as shown in Fig. 2d. Fig. 2a shows the spectrum of the reactor vessel alloy with the blocking shield pulled out, and intense diffraction peaks can be observed. With the blocking shield in place, one obtains almost complete removal of diffraction peaks from both Cr and V edges, as shown in Fig. 2b⁶.

Finally, we tested the ability of the LSR to obtain the Cr XAFS from a sample of 1% Cr in a 99% V matrix. Preliminary tests at the X11 beamline at the NSLS showed that if an ion chamber is used to obtain such data, the V EXAFS oscillations completely overwhelm the Cr absorption edge⁵. We then utilized the PNC-CAT insertion device line at the Advanced Photon Source. This beam was not focused, but nevertheless produced an intensity of $\sim 1 \times 10^{11}$ photons per second in a spot $0.5 \text{ mm} \times 0.5 \text{ mm}$. Fig. 3 shows Cr XAFS obtained for this sample, with background subtracted. At the top one sees the results with the blocking shield removed so that the signal detected by the PIN diodes was partly monochromatized by the LSR and partly direct fluorescence. At the bottom one sees the spectrum with the blocking shield in place. Both the top and bottom of this figure represent identical beam conditions, ten scans averaged. One sees in Fig. 3 a distinct improvement in the signal quality and removal of distortion in regions A and B due to monochromatization by the LSR⁵.

For best quality bulk HOPG, Sparks has shown that one can approach 50% reflection efficiency at the Cu K_α line with a mosaic spread of ~ 0.4 degrees⁷. We have performed diffraction studies on the 0.2 mm-thick flexible HOPG used in our LSR which indicate a peak reflectivity about half that of bulk HOPG at the Cu K_α line and a mosaic spread slightly greater than twice that of best quality HOPG. However, we find that 0.05 mm-thick HOPG has a peak reflectivity only slightly less, and an energy resolution about twice as good as the 0.2 mm-thick material⁶. We could increase the brightness of our LSR by extending the log spiral to accept rays with greater polar angles relative to the sample surface, while not depending on glancing emergent angle rays. The sample self absorption would decrease and the total solid angle would increase. Use of an annular ion chamber, rather than PIN diodes, would insure that all rays reflected from the HOPG would correspond to detectable photons. A helium path would increase intensity at the Cr K edge by a factor of ~ 2 .

The resolution could probably be improved by use of thinner HOPG to approach 130 eV for the Cr K edges. The LSR is not very tunable and requires an intense incident beam in a small spot size. On the other hand, a series of LSR monochromators could be manufactured to cover the first transition row series for less cost than that of a 13 element energy dispersive detector.

References

1. E.A. Stern and S.M. Heald, "An X-ray Filter Assembly for Fluorescence EXAFS Measurements," *Nuclear Instruments and Methods* 172, 397, 1980.
2. M. de Broglie and F.A. Lindemann, *Compt. Rend.*, 158, 944, 1914
3. A.A. Antonov, V.B. Baryshev, I.G. Grigorieva, G.N. Kulipanov, and N.N. Shchipkov, *Nuclear Instruments and Methods in Physics Research A* 308, 1991.
4. J.B. Hastings, M.J. Perlman, P. Oversluizen, P. Eisenberger, and J. Brown, 5th annual SSRL Users Group Meeting, 1978, SSRL Rept. No. 78 - 09.
5. D.M. Pease, M. Daniel, J.I. Budnick, T. Rhodes., M. Hammes, D.M. Potrepka, K. Sills, C. Nelson, S. Heald, D.L. Brewster, A. Frenkel, I.A. Grigorieva, and A.A. Antonov, "Log Spiral of Revolution Highly Oriented Pyrolytic Graphite Monochromator for Fluorescence X-ray Absorption Edge Fine Structure," *Rev. Sci. Instr.* 71, 9, 3267, 2000.
6. D.M. Pease, M. Daniel, J.I. Budnick, B. Taylor, A. Frenkel, K. Pandya, I.K. Grigorieva, and A.A. Antonov, "Extension of a Tuned Log Spiral of Revolution Fluorescence XAFS Detector, Designed for Optimal Detection of a Particular Element Z, to EXAFS of Elements Other Than Z," Accepted, *J. Synchrotron Radiation*
7. C.J. Sparks, Metals and Ceramics Division, Oak Ridge National Laboratory, Annual Progress Report, ORNL-3970, 1966, 57.

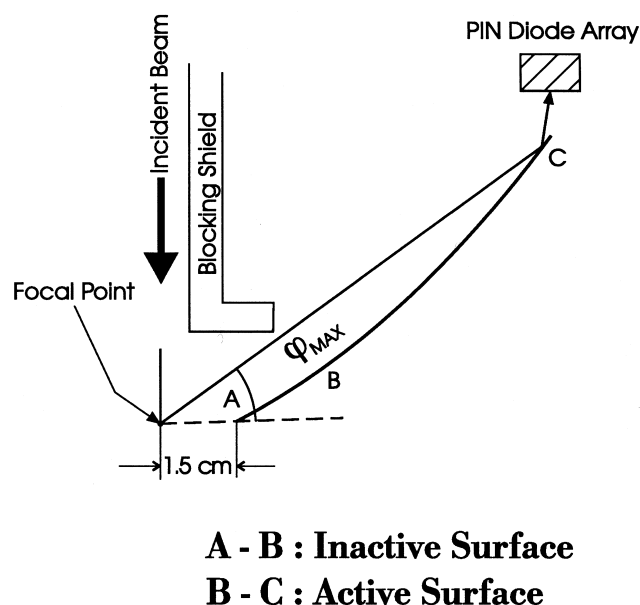


Figure 1. Schematic drawing of a section through a log spiral manufactured for detecting Cr K_{α} . In the version of the log spiral discussed in this manuscript, the active (B-C) area of the surface (i.e., the surface covered with HOPG) begins at zero polar angle. The polar angle ϕ shown corresponds to the maximum polar angle possible for Cr radiation if the active surface begins at zero polar angle.

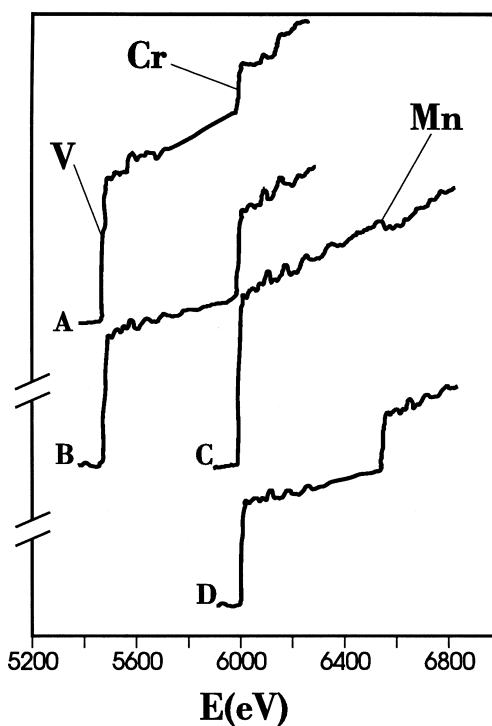


Figure 2. Curve A) LSR set to transmit both V and Cr edges of a $V_{.80}Cr_{.15}Ti_{.05}$ alloy, blocking shield removed to allow transmission of diffraction peaks; Curve B) same as A but with blocking shield in place to remove diffraction peaks; Curve C) $Cr_{.80}Mn_{.20}$ alloy XAFS, LSR tuned to transmit Cr but reject Mn K_{α} ; Curve D) same as C but with LSR tuned to transmit both Cr and Mn K_{α} . The short horizontal lines to the lower left of the four absorption edges represent zero intensity. This level is within uncertainties in the zero adjustment for the PIN diode electronics for the $Cr_{.80}Mn_{.20}$ data sets.

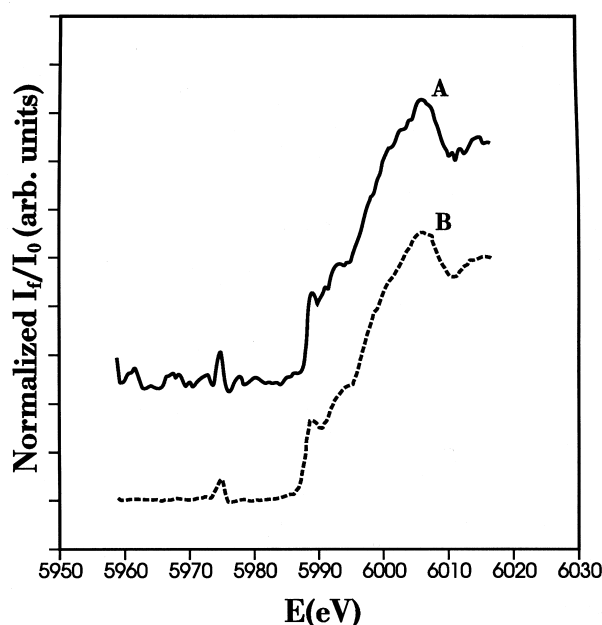


Figure 3. XAFS of Cr in $V_{99}Cr_{01}$, blocking shield out (top) versus blocking shield in (bottom). Background subtracted. Both data sets are ten averaged scans; identical beam conditions for both the blocking shield out and in conditions. Regions denoted by A and B are distorted in shape in the curve taken with the blocking shield out. If the background were not subtracted, the pre-edge background would exhibit an upward slope with increasing energy. The slope of the background observed for data obtained without the blocking shield is much larger than the slope of the background observed with the blocking shield in place. The background just before the edge is reduced by a factor of at least five relative to the Cr absorption step height by the use of the blocking shield. However, the analysis of the true background rejection is complicated by the fact that, even with the blocking shield removed, some signal is monochromatized by the log spiral. Also, there may be detector saturation effects when the blocking shield is removed.

VUV Circular Polarizer: first tests at U5UA

*J.-G. Baek, D. Carlson, Q.Y. Dong, S. Hulbert, G. Nintzel, and
E. Vesco*

National Synchrotron Light Source, Brookhaven National Laboratory, Upton, New York

In recent years, the availability of circularly polarized light (CPL) at synchrotron radiation sources has constantly increased to meet the rising demand for CPL by various spectroscopic techniques. In particular, CPL has been successfully applied to investigations of magnetic materials, mainly taking advantage of magnetic circular dichroism effects.

For more than two decades, circular-polarized soft x-rays ($h\nu = 500\text{--}1500\text{ eV}$) have been extracted from synchrotron sources by collecting the out-of-plane radiation produced by bending magnets. A number of interesting absorption edges of magnetic materials, e.g. the L edges of 3d transition metals and the N edges of the rare earths, fall in this energy range. Consequently, a great amount of absorption and reflectivity work has been performed, particularly on thin films and

multilayers. A great advantage of this type of experiment is the relatively low photon flux required.

The advent of third generation light sources has further expanded the availability of CPL, in particular via the production of CPL by new insertion devices of novel design. The photon flux and brightness of these new sources is much greater than that from out-of-plane bending magnets. Consequently, more demanding experiments, e.g. photoemission and microscopy, have become practically possible. However, the energy range usually covered by these new sources is still centered in the soft x-ray region.

These high photon energies are not suitable for angle-resolved photoemission (ARPES), an experiment typically performed in the photon energy range 10-100 eV. Recently, it has been suggested that an efficient

way to produce CPL at these low energies is to convert linearly polarized light into circularly polarized light by optical methods. Starting from linearly polarized light, typically from an undulator device, the polarization of the emitted light is altered by reflections from a sequence of plane mirrors. At each reflection, owing to the different reflectivities for *s*- and *p*-polarized light, a relative phase shift is introduced between these two components. By appropriate choice of the incident polar (θ) and azimuthal (α) angles, the accumulated phase shift can be made exactly $\lambda/4$, i.e. the transmitted light can be completely circularly polarized¹. This possibility has been experimentally demonstrated at the Synchrotron Radiation Center in Madison, WI². Owing to higher reflectance, the multiple-reflection polarizer is particularly effective in the low energy region of the VUV spectrum (10-50 eV). This is also the most useful photon energy range for ARPES.

In this report, we describe the addition of circular polarization capability to the existing U5UA beamline at NSLS. The U5UA undulator beamline is an intense and highly linearly polarized VUV light source in the photon energy range 10-200 eV. This beamline, and its purpose-built endstation for valence band spin-resolved photoemission spectroscopy, are dedicated to the investigation of the electronic structure of magnetic surfaces and thin films. The addition of circular polarization at U5UA will enable new research programs to be undertaken. Specifically, the addition of circular polarization capability will permit the so-called *complete* photoemission experiment to be performed, in which the polarization of both the incoming (photon) beam and the outgoing (electron) beam are under experimental control. This will have several applications in the spectroscopic investigation of solids. For example, the spin-polarized electronic structure of antiferromagnetically ordered materials will become measurable. Furthermore, the use of CPL will introduce a preferential axis in the experiment so that even paramagnetic materials, previously inaccessible to spin-polarized photoemission, will now become experimentally accessible.

In the last few months, a quadruple-reflection VUV circular polarizer³ has been installed at the U5UA beamline. This polarizer consists of two pairs of mirrors arranged in a symmetric, trombone geometry as shown in Fig.1. The use of four consecutive mirrors provides a very convenient solution for use in a synchrotron radiation beamline in that the outgoing (circular-polarized) beam has the same direction as the incoming (plane-polarized) beam.

According to the Fresnel equations, the reflectances for *p*- and *s*-polarized light incident on a plane mirror with dielectric constant $\epsilon(h\nu)$ at a grazing incident angle θ are

$$r_p e^{i\delta_p} = \frac{\epsilon \sin\theta - \sqrt{\epsilon - \cos^2\theta}}{\epsilon \sin\theta + \sqrt{\epsilon - \cos^2\theta}} \quad \text{and}$$

$$r_s e^{i\delta_s} = \frac{\sin\theta - \sqrt{\epsilon - \cos^2\theta}}{\sin\theta + \sqrt{\epsilon - \cos^2\theta}}. \quad (1)$$

After a single reflection, the phase shift Δ_1 between *p*- and *s*- reflected light is $\Delta_1 = \delta_p - \delta_s$. The first of two conditions needed to obtain purely circular polarized light after four consecutive reflections is given by

$$\Delta_{tot} = 4\Delta_1 = \pm \frac{\pi}{2}. \quad (2)$$

Additionally, for a purely linearly polarized beam of amplitude I_0 incident on the polarizer at an azimuthal angle α (see Fig. 2), the second condition needed to produce circular polarized light is

$$\begin{aligned} (I_0 \sin\alpha) r_s &= (I_0 \cos\alpha) r_p \\ \Rightarrow r_p &= r_s \tan\alpha \\ \Rightarrow \alpha &= \tan^{-1}\left(\frac{r_p}{r_s}\right) = \tan^{-1}\left(\frac{r_{p1}}{r_{s1}}\right)^4 \end{aligned} \quad (3)$$

Simultaneous solution of Eqs. (2) and (3) yields the values of α and θ which produce pure CPL for each photon energy⁴. Assuming 100% linearly polarized incident light, the calculated $(\alpha, \theta)^{cir}$ curves for 100% circular polarized output are shown in Fig. 3 (dashed lines) for the 10-70 eV photon energy range. In our case, the circular polarizer is not the last optical element in the beamline. Rather, for space reasons, it is mounted just before the last refocusing (Au coated) mirror M_1 , whose grazing angle of incidence is 5° . The presence of M_1 (not shown in Fig.1) slightly modifies the optimum $(\alpha, \theta)^{cir}$ values. The corrected values are also shown in Fig. 3 (solid lines).

The calculated polarization can be experimentally verified by analyzing the polarization of the light after the polarizer. Our analyzer consists of a plane mirror and a rigidly connected VUV-sensitive photodiode⁵ located downstream of the quadruple reflection polarizer (see Fig. 1). The angle of incidence on the plane mirror is 45° and the entire analyzer can be rotated around

the photon beam axis by an angle ϕ while the diode intensity is being monitored. Since the reflectivity of the 45° angle-of-incidence Au mirror for s-polarized light is much higher than for p-polarized light, we can selectively measure the intensity of the s-polarization component with this mirror. With pure linearly polarized light, we expect to measure an oscillation in the intensity of the light as a function of ϕ from a maximum for purely s-polarized reflection geometry to a minimum for purely p-polarized reflection geometry. In the special case of pure circular polarized light, the photodiode intensity should be independent of ϕ . By minimizing the photodiode intensity oscillations vs. ϕ , the experimental values for the optimum $(\alpha, \theta)^{\text{cir}}$ can be established.

The experimentally determined $(\alpha, \theta)^{\text{cir}}$ values are shown in Fig. 3 (dots) in the photon energy range 20–70 eV. Although one can see a general agreement between theory and experiment, there are significant differences. The experimental θ values suffer a nearly constant offset of about 2° with respect to the calculated values. Furthermore, above 35 eV the measured α values are significantly smaller than expected from theory. The origin of these differences is not completely clear at the moment. Part of the answer must be the presence of second and higher order diffracted light from the grating, located upstream of the polarizer. The U5UA beamline design is optimized for high photon flux, the major limiting factor in spin-resolved photoemission experiments, at the expense of spectral purity.

Note that although the differences between calculated and measured $(\alpha, \theta)^{\text{cir}}$ shown in Fig. 3 can affect the efficiency of the polarizer, they do not affect the degree of circular polarization of the light, which can still be 100%. This can be best appreciated by looking

at the polar plots of photodiode intensity vs. ϕ shown in Fig. 4, which shows the intensity variations as a function of ϕ for (α, θ) close to the optimum $(\alpha, \theta)^{\text{cir}}$ pure circular polarization values. As the α or θ angle is displaced from $(\alpha, \theta)^{\text{cir}}$ (the perfect circle in each polar plot of Fig. 4, indicated by Δ symbols), a component of linearly polarized light is introduced in the outgoing beam and an oscillation is observed in the photodiode output (i.e. the polar ϕ plots become non-circular). As one would expect, the photodiode intensity is more sensitive to changes in θ while the phase change and, therefore, the degree of circular polarization, is dependent on both α and θ .

An interesting point can be noticed by examining calculated degree-of-circular-polarization contour maps, an example of which is shown in Fig. 5 for 40 eV incident photon energy. It is apparent that the sensitivity to α and θ near 100% circular polarization is not very high. For example, near the optimum values $(\alpha, \theta)^{\text{cir}}$, there is a rather large region of the (α, θ) -plane ($\Delta\alpha \approx 10^\circ$, $\Delta\theta \approx 5^\circ$) where the degree of circular polarization is larger than 95%.

A very important parameter of the polarizer is, of course, its transmission. In our beamline, this parameter is difficult to determine experimentally owing to the presence of higher diffracted orders from the grating as mentioned above. Nevertheless, the theoretical calculations of its transmission are reported in Fig. 6. As one can see, in the low photon energy range (<50 eV), the transmission of the four-reflection circular polarizer is high enough to make it a very useful device.

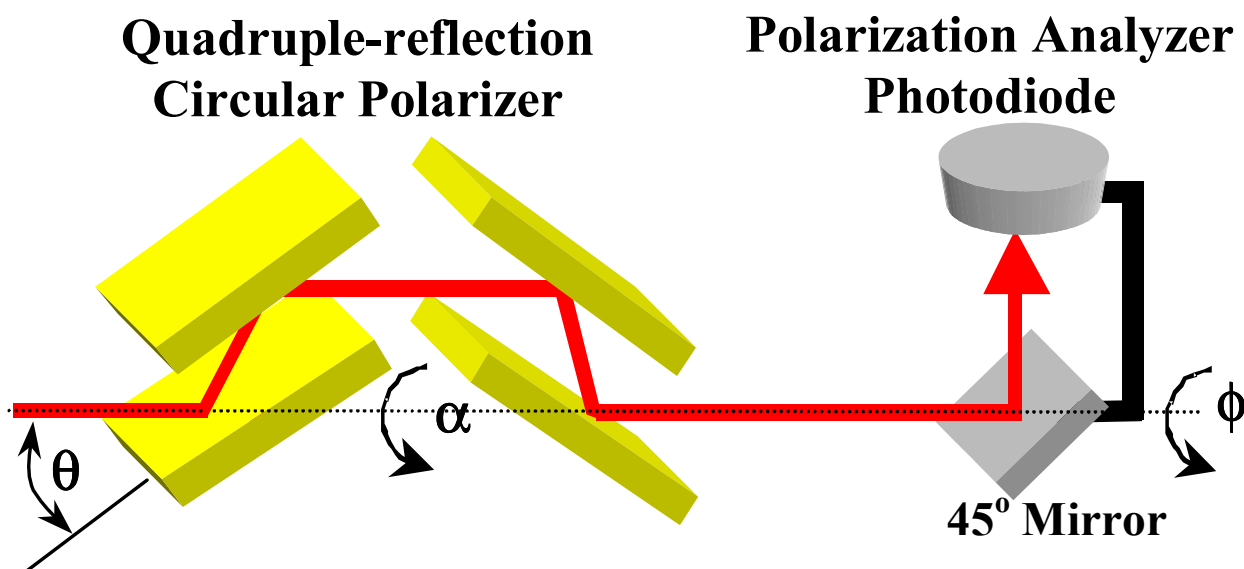


Figure 1. Schematic drawing of the quadruple-reflection polarizer and the polarization analyzer at beamline U5UA.

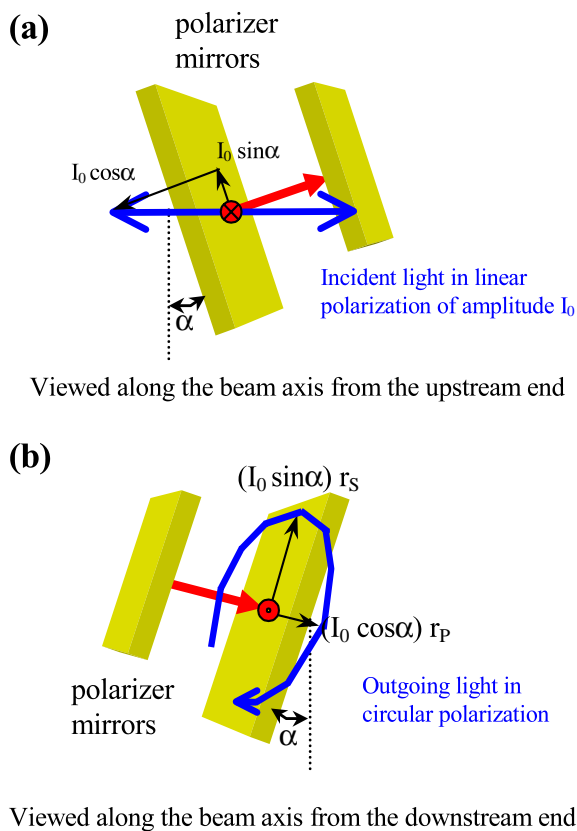


Figure 2. p- and s- components of the photon beam amplitude (a) before and (b) after the quadruple-reflection polarizer.

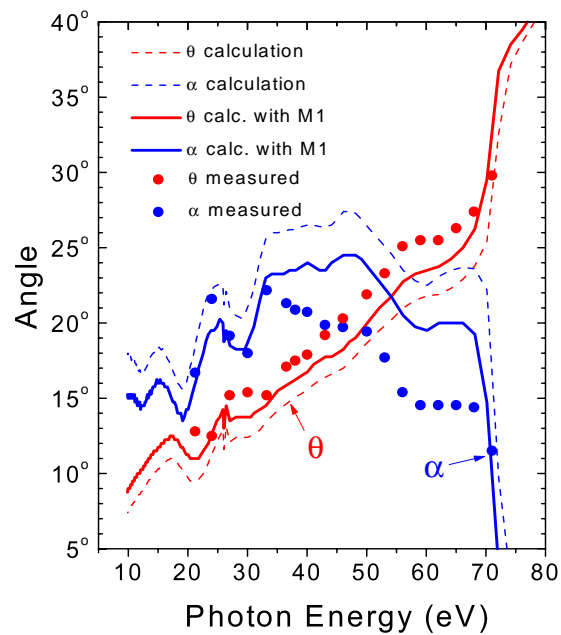


Figure 3. α -, θ -angles for pure circular polarized light as a function of photon energy.

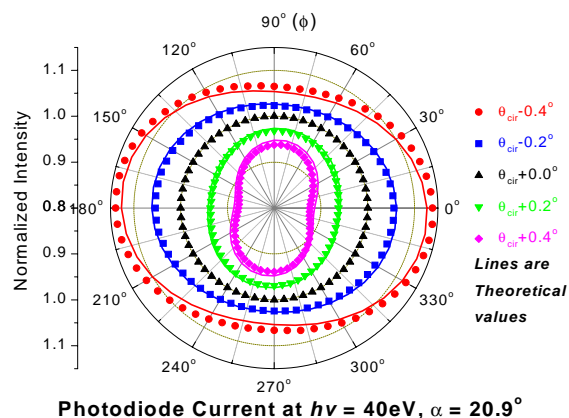
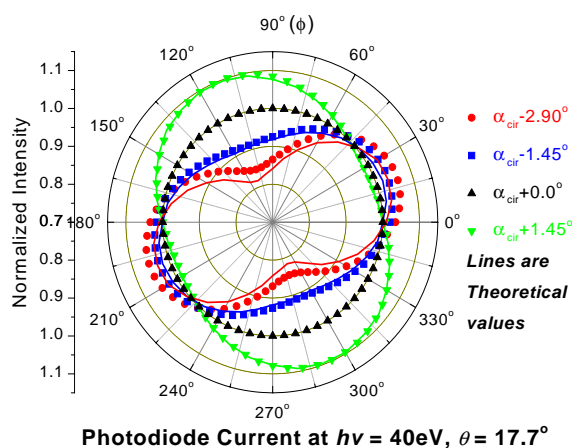


Figure 4. Measured(symbols) and calculated(solid lines) beam intensities as functions of analyzer angle Φ close to the optimum $(\alpha, \theta)^{\text{cir}}$ condition for (a) fixed α -angle and (b) fixed θ -angle.

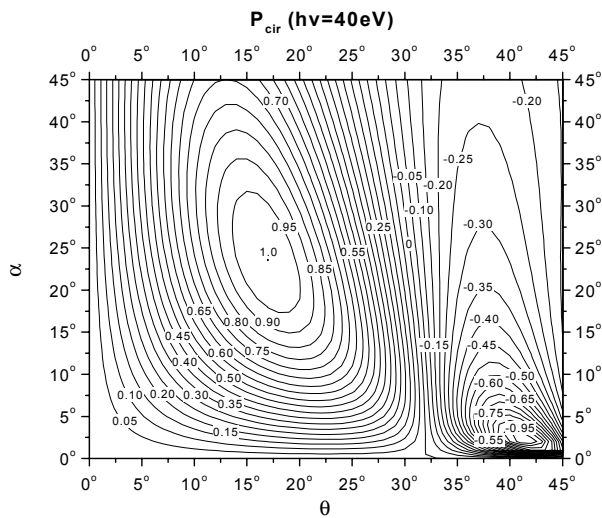


Figure 5. Contour map of calculated circular polarization (P_{cir}) as a function of α - and θ -angles at $h\nu=40\text{eV}$.

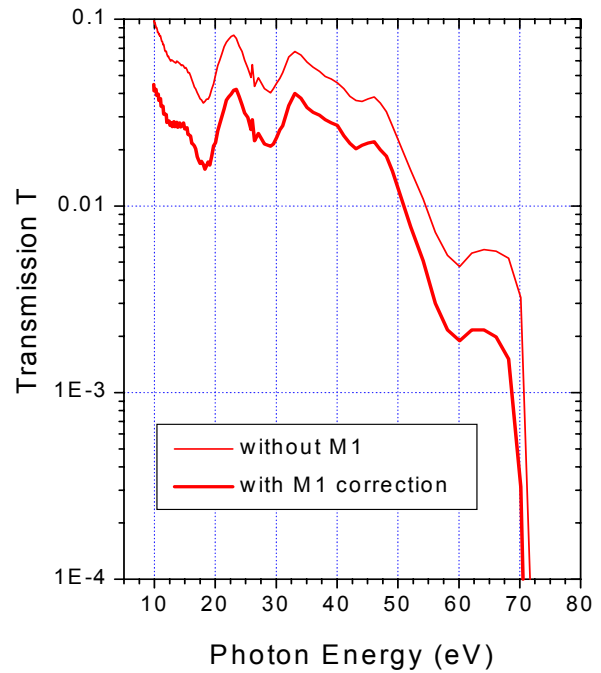


Figure 6. Calculated transmission of the polarizer at the perfect circular polarization condition as a function of photon energy.

References:

- 1 N.V. Smith, P.D. Johnson, Nucl. Instr. and Meth. A **214**, 505 (1983).
- 2 H. Höchst, R. Patel, F. Middleton, Nucl. Instr. and Meth. A **347**, 107 (1994).
- 3 The U5UA circular polarizer was been designed and manufactured at The Physical Sciences Laboratory (PSL) of the University of Wisconsin-Madison.
- 4 E.D. Palik, *Handbook of Optical Constants of Solids*, ed. E.D. Palik, Academic Press, Orlando, 1985.
- 5 International Radiation Detectors, Inc., Torrance, CA. See R. Korde and J. Geist, Applied Optics **26**, 5284 (1987).